JOURNAL OF MATERIALS SCIENCE **38** (2003) 4883–4888

The influence of interfacial dislocation arrangements in a fourth generation single crystal TMS-138 superalloy on creep properties

J. X. ZHANG*, T. MURAKUMO, Y. KOIZUMI, H. HARADA
National Institute for Materials Science, 1-2-1 Sengen, Tsukuba, Ibaraki 305-0047, Japan
E-mail: jian-xin.zhang@nims.go.jp

The morphologies of (001) γ/γ' interfacial dislocation networks are studied through TEM observations. The lattice misfit has an important relation with creep property for superalloy during high temperature creep deformation. The fourth generation superalloy TMS-138 possesses superior creep properties based on its fine interfacial dislocation networks. The networks have two typical characteristics: closely spaced dislocations and stable square morphology during creep deformation. Such arranged dislocations can effectively prevent the slipping dislocations in the γ phase from moving through the γ/γ' interface and improve drastically the creep resistance in the fourth generation superalloy TMS-138.

1. Introduction

Ni-base single crystal (SC) superalloys, which have remarkable mechanical properties at elevated temperatures, have been designed for use as turbine blades in aeroengines. In order to develop higher efficiency engines, considerable efforts have been being devoted to enhance the temperature capabilities of superalloys. In addition to Ni and Al, the superalloys usually contain several alloying elements to enhance creep resistance capability, such as Cr, Co, Mo, W and Ta [1, 2]. Of considerable importance in determining the mechanical properties of superalloys are the γ/γ' interfacial dislocations [3, 4]. The morphologies and roles of these interfacial dislocations have been extensively studied by many researchers [5–13]. However, the description of characteristic dislocation networks in superalloys of superior creep resistance has not been made clearly so far.

In the past two decades, four generations of single crystal (SC) superalloys have been successfully developed in our institute (NIMS, Japan) [14–16]. Our work showed that the temperature capacity is improved by changing the lattice misfit towards greater negativity [14, 17, 18]. With this design guideline, the fourth generation superalloy (TMS-138) has obvious superiority to the third generation (TMS-75) [16]. The main objective of this study is to investigate the featured characteristics of interfacial dislocation networks in a TMS-138 superalloy after creep rupture at 1100°C and 137 MPa. As a comparative, other superalloys related to the third generation alloy TMS-75 with different misfits were also observed to highlight the featured dislocation networks in superalloys.

2. Experimental

The development of the 4th generation superalloy and its related properties were given in reference [16]. Single crystal bars of $\varphi 10 \times 130$ mm were cast with the directionally solidified furnace in the institute. The chemical composition of the alloys is listed in Table I and heat treatments are given as follows

TMS-75:

1300°C/1 h → 1320°C/5 h GFC → 1100°C/4 h GFC → 870°C/20 h GFC

TMS-75(+Ru):

1300°C/1 h → 1320°C/5 h AC → 1150°C/4 h AC → 870°C/20 h AC

TMS-75(+Mo):

1250°C/1 h → 1270°C/1 h → 1290°C/1 h → 1310°C/1 h → 1320°C/2 h → 1340°C/2 h → 1350°C/10 h → 870°C/20 h GFC

TMS-75(+Mo, Ru)(TMS-138):

1300°C/1 h → 1340°C/5 h AC → 1150°C/4 h AC → 870°C/20 h AC

(GFC: Gas Fan Cooling; AC: Air Cooling)

After heat treatments, creep test specimens (4 mm in diameter with 22 mm long gage section) were machined from the single crystal bars. Creep tests were performed in air at 1100°C and 137 MPa. Creep rates

*Author to whom all correspondence should be addressed.

TABLE I Nominal composition of the investigated alloys (wt%)

	Co	Cr	Mo	W	Al	Ta	Hf	Re	Ru	Ni
TMS-75	12	3	2	6	6	6	0.1	5	0	Bal.
TMS-75(+Mo)	6	3	3	6	6	6	0.1	5	0	Bal.
TMS-75(+Ru)	12	3	2	6	6	6	0.1	5	1.6	Bal.
TMS-75(+Mo, Ru) (TMS-138)	6	3	3	6	6	6	0.1	5	2	Bal.

were measured by using non-contact measuring system for high temperature with CCD (Charge Coupled Device) camera so that the measurement was accurate. Two sets of CCD camera systems were used to respectively record the movement of two markers of the specimen during creep. After creep rupture, these specimens were cut to thin slices perpendicular to the [001] direction. Transmission electron microscope (TEM) foils were electrochemically thinned in a solution of 80 ml perchloric acid, 20 ml ethanol and 400 ml 2-Butex ethanol at 3–7°C. A JEM-2000 FX II transmission electron microscope was used for the observation of dislocation configuration. For each superalloy 43 areas were randomly selected to study interfacial dislocation spacing.

3. Results and discussion

3.1. Creep tests at 1100°C and 137 MPa

Fig. 1 shows the creep curves of the four superalloys at 1100°C and 137 MPa. Obviously the fourth generation superalloy TMS-138 has the smallest minimum creep rate and the longest creep rupture life among all of the four superalloys. In contrast, the superalloy TMS-75(+Ru) manifests the largest minimum creep rate and the shortest creep rupture life.

After creep tests the dislocation spacings on the (001) γ/γ' interfacial plane were measured in TEM under a two-beam condition. The relationship of minimum creep rate vs dislocation spacing is shown in Fig. 2. The minimum creep rate is proportional to the interfacial dislocation spacing. This is attributed to the fact that finer interfacial misfit dislocation network can effectively prevent glissile dislocations from shearing into γ' phase or moving out of γ' phase. It is well known that interfacial dislocation spacing is inversely proportional to the misfit between the γ and γ' phases [8].

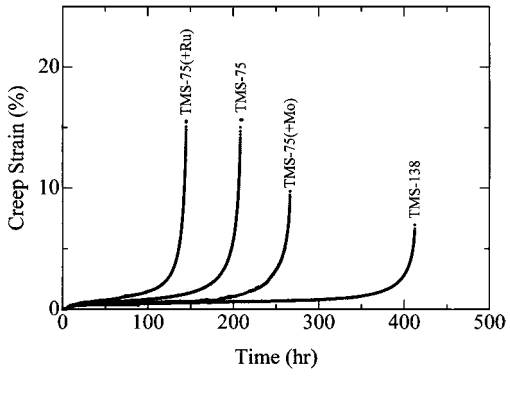

Figure 1 Creep curves of TMS-75, TMS-75(+Mo), TMS-75(+Ru), and TMS-138 single crystals tested at 1100°C and 137 MPa.

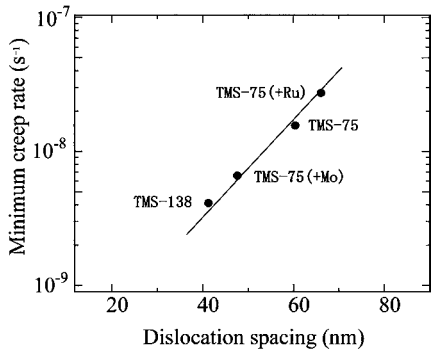

Figure 2 Minimum creep rates of TMS-75, TMS-75(+Mo), TMS-75(+Ru), and TMS-138 as a function of their interfacial dislocation spacing.

Therefore the creep tests verify that lattice misfit is one of the important factors, which affect the creep properties at high temperatures.

3.2. Distribution of γ/γ' interfacial dislocations

Fig. 3 shows the distribution of interfacial dislocation spacings in the four superalloys. These results are very interesting and comparable. The interfacial dislocation spacing in TMS-75(+Ru) is distributed in a wide range from 46 to 86 nm (Fig. 3a). Comparatively, the dislocation spacing in TMS-138 is restricted to a narrow range of 32–50 nm and mainly concentrated near by its mean value of ~41 nm (Fig. 3d). In general, with the increase in negative misfit, the interfacial dislocation spacing approaches the value determined by the lattice misfit. Comparing to the dislocation distribution in TMS-75(+Ru) or TMS-75, the mean dislocation spacing in TMS-75(+Mo) is shifted leftward to lower values (~47 nm). This trend is more obvious in the fourth generation superalloy TMS-138, because many of the interfacial dislocations have the mean spacing ranging from 40 to 42 nm. From this point, the interfacial dislocations are most uniformly distributed in the fourth generation superalloy TMS-138.

When a moving dislocation bypasses the interfacial dislocation network, the shear stress required to pass it is inversely proportional to the curvature radius of the dislocation segment intersected by interfacial network

$$\tau = \frac{Gb}{2r}$$

where τ and r are the shear stress and curvature radius, respectively. The critical stress is also inversely proportional to the dislocation spacing. Thus, under the same tensile stress, the interfacial dislocation network with a large spacing can not effectively prevent the glissile dislocations in the γ channel from bypassing the interface. In this sense, TMS-138 has more sturdy dislocation networks (a mean spacing of 41 nm) than the other three superalloys TMS-75(+Mo) (47 nm), TMS-75 (61 nm) and TMS-75(+Ru) (65 nm).

Besides understanding the role of effective impeding dislocation movement by the interfacial dislocation networks, based on the concept of a mean value of

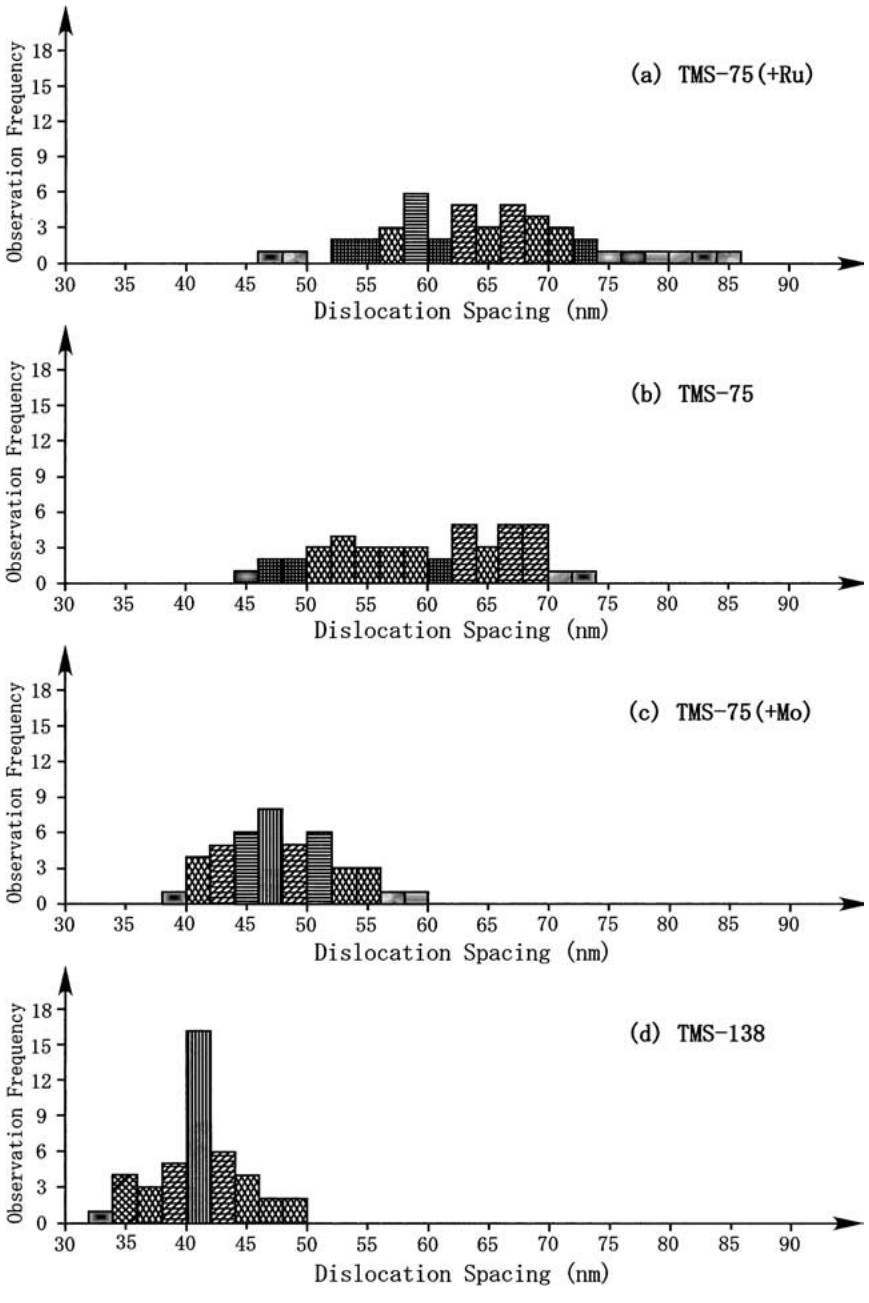

Figure 3 Distribution of γ/γ' interfacial dislocations.

dislocation spacing shown in Fig. 2, the distribution of interfacial dislocations is also very important to assess this kind of prevention. For example, although the mean dislocation spacing in TMS-75(+Ru) is ∼65 nm, considerable number of dislocations exists with spacings in the range of 70–86 nm. For these large-spaced interfacial dislocations, glissile dislocations in the γ matrix can easily pass through them and shear the rafted γ' phase. In other words, the interfacial dislocations in TMS-138 are distributed homogeneously and can effectively prevent the dislocation glide in the γ channel.

The dislocations within the networks are thought to originate from the matrix glissile dislocations captured on the interface. However, the ⟨110⟩ directions of the dislocation lines deposited on the interfaces are not in the proper orientation to efficiently relieve the mismatch [19]. The orientation change from slip (along ⟨110⟩) to mismatch (along ⟨100⟩) involves the formation of Orowan loops around the γ' particles. These loops must subsequently rotate by 90° along the γ/γ' interface, by a combination of glide and climb, in order to orient themselves to the most efficient relieve of the mismatch strains [20].

Our recent work and previous research by other workers show that these mismatch interfacial dislocations are edge in character and have Burgers vectors corresponding to octahedral slip, i.e., $b = 1/2[011]$, $1/2[01\bar{1}]$, $1/2[101]$ and $1/2[10\bar{1}]$ [8, 12, 21]. These vectors are angled by 45° to the γ/γ' (001) interface plane and thus such dislocations are sessile [8]. That is why, after reorientation of interfacial dislocations from ⟨110⟩ to ⟨100⟩, the possible movement of dislocations can only be accomplished by climb. Fig. 4 is the schematic illustration of interfacial dislocation rows along the [100] direction. These dislocations have Burgers vectors $b_1 = 1/2[011]$ and $b_2 = 1/2[01\bar{1}]$, and every dislocation has the Burgers vector different from its two neighboring ones. The dislocation line

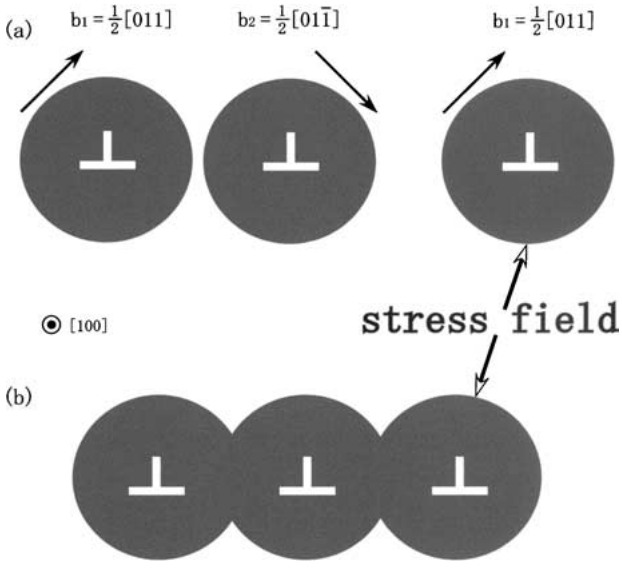

Figure 4 Schematic illustration showing variable dislocation spacing due to dislocation interaction. (a) Small misfit resulting in large dislocation spacing and weak interaction between dislocations. (b) Large misfit resulting in small dislocation spacing and strong interaction between dislocations.

is perpendicular to its corresponding Burgers vector. Meanwhile, the Burgers vector b_1 is perpendicular to the b_2. It is well known that two dislocations with Burgers vectors with the same sign will repel mutually. However, in the present situation the interaction between two dislocations with different Burgers vectors is very complex. Although these interfacial dislocations are sessile, at so high temperature (1100°C) they may move by the diffusion-related climb. According to the theory of dislocations [22], the interaction force between two dislocations is inversely proportional to their spacing. The dislocations with large spacing may exhibit a weak interaction and can move in a relatively large range (Fig. 4a). In TMS-75(+Ru) the dislocation spacing determined by lattice misfit is 65 nm approximately. Some dislocations may move by climb to form dislocations closely spaced or loosely arranged in some area. In contrast, dislocations with small spacing in TMS-138 can not move considerably out of their well-defined positions by lattice misfit because their interaction force is strong (Fig. 4b). That is why the interfacial dislocations are distributed so homogeneously in TMS-138. It must be pointed out that this kind of adjustment of the dislocation spacing by climb is a local process and it is caused by the local strain field. On average, the dislocation spacing keeps basically constant during the secondary creep stage as it was observed and determined by Gabb *et al.* [8] by the mismatching between the γ and γ' phases.

Generally speaking, interfacial dislocations consist of two rows of dislocations in two mutually perpendicular directions, i.e., [100] and [010]. Fig. 4 shows only one row of such dislocations in the [100] direction. The other row of dislocations is arranged along the [010] direction (which can be found in the same way). Those dislocations have Burgers vectors $b_3 = 1/2[101]$ and $b_4 = 1/2[10\bar{1}]$. That row of dislocations exhibits the similar interaction behavior to the former one discussed earlier.

3.3. Morphology of γ/γ' interfacial dislocation networks

Fig. 5 shows the γ/γ' interfacial dislocation networks in TMS-138 (a), TMS-75(+Mo) (b), TMS-75 (c) and TMS-75(+Ru) (d) after creep rupture. The electron beam is nearly perpendicular to the macroscopic γ/γ' interfacial plane (001). In general, the dislocation lines in superalloys TMS-138 and TMS-75(+Mo) are straight. The typical morphologies of the interfacial dislocation networks in these two alloys are roughly square networks, as in the area marked by squares in Fig. 5a and b. Relative to the straight dislocation lines in the sample TMS-138 or TMS-75(+Mo), the dislocations in Fig. 5c and d show obviously a wave-like characteristic. It seems that the dislocation networks in TMS-75 (Fig. 5c) and TMS-75(+Ru) (Fig. 5d) have suffered from more serious deformation than those in Fig. 5a and b. As stated above, dislocations aligned in ⟨100⟩ directions can effectively accommodate misfit between the γ and γ' phases. Thus, we can imagine that during the early stage of creep the misfit dislocations are well arranged along [100] and [010] directions and form regular square networks. During creep, two kinds of phenomena occur for these dislocations. One is the possible climb shown by the curved dislocation lines in Fig. 5c and d. Since the Burgers vectors are angled at 45° to the (001) interface planes, the misfit dislocations are sessile. During high temperature creep (1100°C), such dislocations may move by climb to response to external tensile stress. The other phenomenon is the formation of new dislocation nodes. The old node and the newly formed one are connected by a new dislocation segment. These new dislocation segments are edge in character and lie along [110] or [1$\bar{1}$0] direction with Burgers vectors 1/2[1$\bar{1}$0] or 1/2[110], respectively. Such typical configurations are marked by circles in Fig. 5c and d.

Fig. 6 shows an ideal model for the evolution of dislocation networks during the secondary creep stage in the superalloys. For the small-spaced dislocation networks in the TMS-138 or TMS-75(+Mo) alloys, the initial square-like configuration can be basically kept during the creep test. For the large-spaced dislocation networks in the TMS-75 or TMS-75(+Ru) alloys, the initial interfacial misfit dislocation networks are also square in shape, as shown in Fig. 6a. However, formation of a new dislocation node is possible by one of the following dislocation reactions.

$$\frac{1}{2}[10\bar{1}] + \frac{1}{2}[011] \rightarrow \frac{1}{2}[110] \quad (1)$$

$$\frac{1}{2}[101] + \frac{1}{2}[01\bar{1}] \rightarrow \frac{1}{2}[110] \quad (2)$$

$$\frac{1}{2}[10\bar{1}] + \frac{1}{2}[0\bar{1}1] \rightarrow \frac{1}{2}[1\bar{1}0] \quad (3)$$

$$\frac{1}{2}[101] + \frac{1}{2}[0\bar{1}\bar{1}] \rightarrow \frac{1}{2}[1\bar{1}0] \quad (4)$$

These resultant dislocation segments lie in the [110] or [1$\bar{1}$0] direction with Burgers vector $b = 1/2[1\bar{1}0]$ or $b = 1/2[110]$ (as shown in Fig. 6b). Therefore, these segments are edge in character. The Burgers vectors

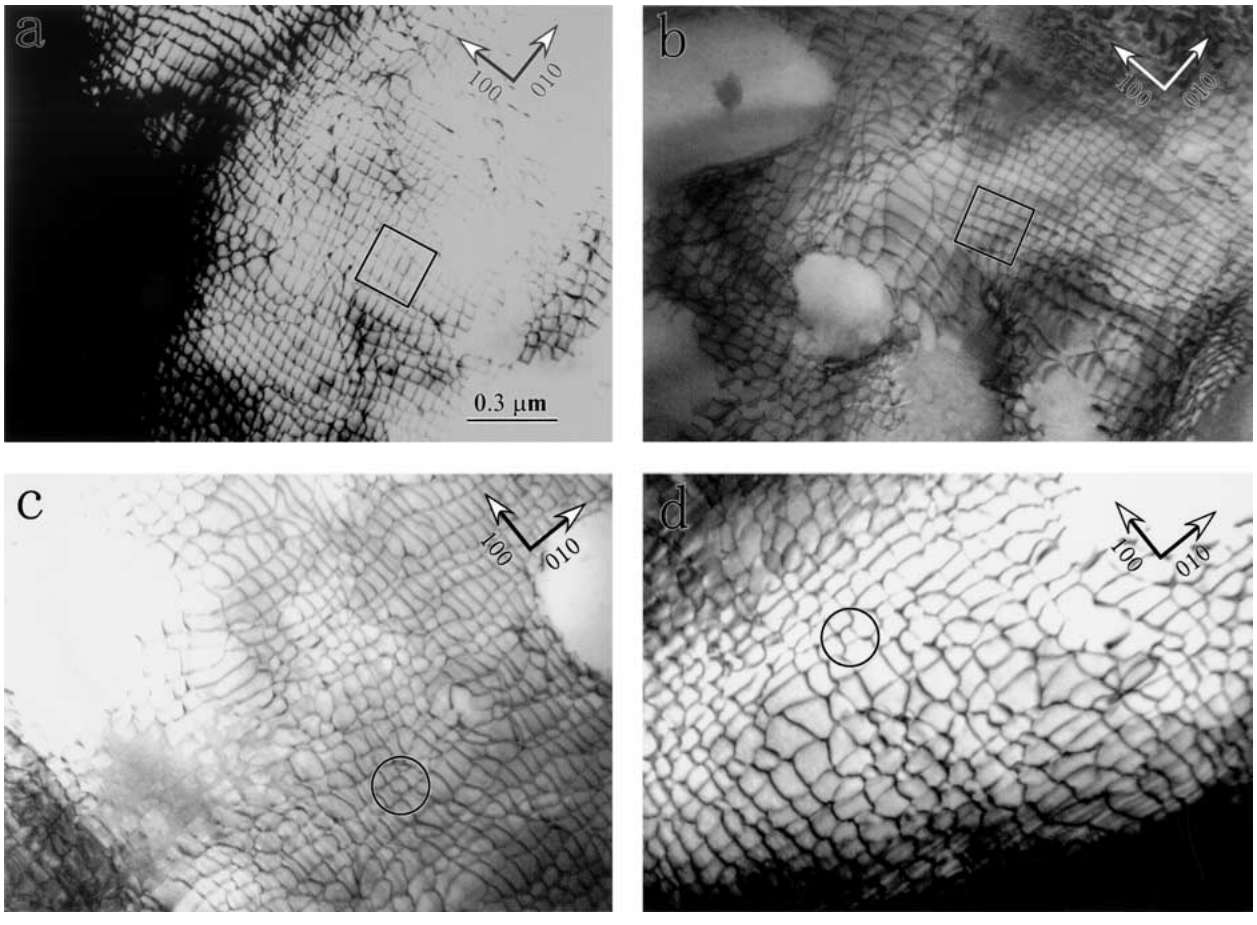

Figure 5 Morphology of the interfacial dislocation networks in (a) TMS-138, (b) TMS-75(+Mo), (c) TMS-75 and (d) TMS-75(+Ru). The typical regularity of dislocation networks are enclosed by squares in (a) and (b). A mesh is connecting with its neighbors by new-formed segments in the circled area in (c) and (d).

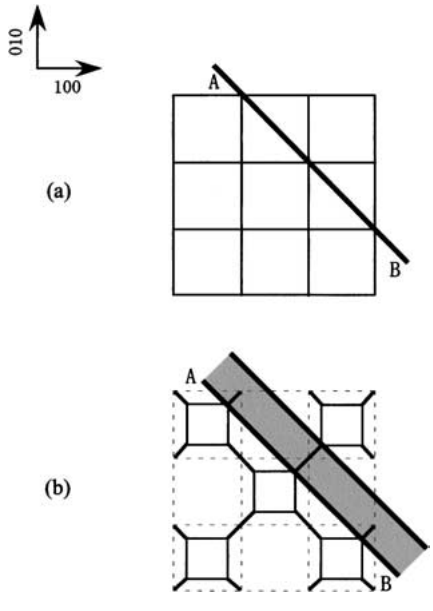

Figure 6 Schematic illustration of the evolution of dislocation network during creep deformation: (a) Regular arrangement of interfacial dislocations. The interfacial dislocation network is intersected by a glissile dislocation AB with the Burgers vector $b = 1/2\langle 101\rangle$. (b) Dislocation reactions at nodes change the shape of the network (dashed lines stand for dislocation lines before dislocation reactions). If the dislocation AB in the diagonal line in (a) is the only dislocation which can pass through the interface, the possibility for the glissile dislocation to pass is considerably increased after the dislocation reaction as shown by the shadowed area in (b).

of these new dislocations are in the (001) interfacial plane and can effectively accommodate misfit strain between the γ and γ' phases. The reaction from the left to the right in Equations 1–4 results in decreasing of $|b^2|$ from a^2 to $1/2a^2$ (where a is the lattice parameter) and thus is energetically favorable. On the other hand, the formation of these new dislocation segments would lead to diminishing of some dislocation network meshes, as shown in Fig. 6b, by the change from original dislocation network frame (dashed line) to the resultant dislocation network (solid line). The diminishing of mesh size means the increase of repulsive force between two parallel dislocation lines in a mesh. As discussed above, large-spaced dislocation networks allow the dislocations to move by climb in a larger range than the small-spaced ones do. Altogether, large-sized dislocation network meshes would diminish more obviously than the small-sized ones, which is manifested by the well-defined new dislocation segments.

The formation of new segments by dislocation reactions during creep will result in an increased possibility of a glissile dislocation in γ channel to pass through these interfacial dislocation networks. For example, a glissile dislocation AB is moving to the interfacial dislocation network along the diagonal line of the rectangular mesh (Fig. 6a). The diagonal line is the most possible position for the glissile dislocation to penetrate the network meshes in the interface, because the slipping dislocation has its longest segments within the mesh

when intersecting the dislocation networks. Obviously, after dislocation reactions, the possibility for glissile dislocations to pass through the interface is increased significantly as marked by the gray area in Fig. 6b.

Another process accompanying high temperature creep is the dislocation lines' curving as shown in Fig. 5c and d. These characteristic curves represent an occurrence of climb or slip. Because these interfacial dislocations are sessile, slip of dislocations can be excluded. It is very likely that high temperature climb results in the formation of these curved dislocation lines. The curved γ/γ' interfacial dislocation networks may act as the source of glissile dislocations. For the regular square networks, the dislocations are in edge character, and their Burgers vectors are not lying in the interface plane. Therefore, these dislocations cannot glide neither in the plane {001} in which the dislocation lies, nor in the {111} planes in which the Burgers vectors lie. However, after bending the dislocation lines deviate from their original [100] or [010] directions. Some segments may become parallel to [110] or $[1\bar{1}0]$. Thus, these segments can slip on the {111} planes again. The study on interfacial dislocations acting as dislocation source to cut γ' phase during high temperature creep is under way by *in situ* observation in our research group.

As discussed above, the process related to the formation of new dislocation segments and curving of dislocation lines does not change the interfacial dislocation spacing on average. However, these changes (dislocation reactions and curving) may become, to a certain extent, detrimental to creep deformation. Therefore, a set of dense and stable interfacial dislocation networks is very important for the creep process of superalloy.

In TMS-138 and even in TMS-75(+Mo), their interfacial networks are stable and thus these two superalloys exhibit low minimum creep rates and long creep rupture life. In fact, the fourth generation superalloy TMS-138 has larger interface area than TMS-75(+Mo). This area contains square-like dislocation networks, though curving of interfacial dislocations can be also found in some areas of these two alloys. This fact shows that TMS-138 has lower minimum creep rate and longer rupture life than TMS-75(+Mo). As far as TMS-75 or TMS-75(+Ru) alloys are concerned, their unstable interfacial dislocation networks make a contribution to their high minimum creep rate and short creep rupture life relative to the fourth generation superalloy TMS-138.

4. Conclusions

The following conclusions could be drawn out from this study.

1. The lattice misfit is a vital factor which affects the creep properties at high temperature. During high temperature creep, the misfit can be relieved by formation of interfacial dislocation networks between the γ and γ' phases.

2. The fourth generation superalloy TMS-138 has finer interfacial misfit dislocation networks. These interfacial dislocations can effectively prevent the shear of the γ' phase by glissile dislocations in the γ channel.

3. The interfacial dislocation networks in TMS-138 are stable and can keep its original square-like shape during creep deformation at high temperature, while widely spaced dislocations at the interfaces in the third generation superalloy, such as TMS-75, may locally adjust their spacing by the reaction between dislocations or curving and further widen locally during steady creep stage. These changes in dislocation configurations may increase the possibility for slipping dislocations in the γ phase to move into or out of the γ' phase through the interface.

References

1. F. R. N. NABARRO and H. L. VILLIERS, "The Physics of Creep" (Taylor & Francis, London, 1995) p. 174.
2. C. T. SIMS, N. S. STOLOFF and W. C. HAGEL, "Superalloys II" (John Wiley & Sons, New York, 1987) p. 97.
3. H. HARADA, M. YAMAZAKI and Y. KOIZUMI, *Tetsu to Hagane* (in Japanese) **65** (1979) 1049.
4. Y. RO, Y. KOIZUMI and H. HARADA, *Mater. Sci. Eng.* A **223** (1997) 59.
5. G. C. WEATHERLY and R. B. NICHOLSON, *Phil. Mag.* **17** (1968) 801.
6. A. LASALMONIE and J. L. STRUDEL, *ibid.* **32** (1975) 937.
7. T. LINK and M. FELLER-KNIEPMEIER, *Z. Metallkde.* **79** (1988) 381.
8. T. P. GABB, S. L. DRAPER, D. R. HULL, R. A. MACKAY and M. V. NATHAL, *Mater. Sci. Eng.* A **118** (1989) 59.
9. T. M. POLLOCK and A. S. ARGON, *Acta Metall. Mater.* **40** (1992) 1.
10. R. R. KELLER, H. J. MAIER and H. MUGHRABI, *Scripta Metall. Mater.* **28** (1993) 23.
11. R. VOLKL, U. GLATZEL and M. FELLER-KNIEPMEIER, *ibid.* **31** (1994) 1481.
12. V. SASS and M. FELLER-KNIEPMEIER, *Mater. Sci. Eng.* A **245** (1998) 19.
13. M. KOLBE, A. DLOUHY and G. EGGELE, *ibid.* **246** (1998) 133.
14. H. HARADA and H. MURAKAMI, "Springer Series in Materials Science" (Springer-Verlag, Berlin Heidelberg, 1999) p. 39.
15. H. HARADA, The 2nd International Symposium, "High Temperature Materials 2001," National Institute for Materials Science, 2001, p. 4 (submitted to Mater Sci Eng).
16. Y. KOIZUMI, T. KOBAYASHI, T. YOKOKAWA and H. HARADA, The 2nd International Symposium, "High Temperature Materials 2001," National Institute for Materials Science, 2001, p. 30 (submitted to Mater Sci Eng).
17. H. HARADA, K. OHNO, T. YAMAGATA, T. YOKOKAWA and M. YAMAZAKI, in "Superalloys 1988" edited by S. Reichman *et al.* (Metallurgical Society, 1988) p. 733.
18. H. HARADA, T. YAMAGATA, T. YOKOKAWA, K. OHNO and M. YAMAZAKI, in Proc of 5th International Conference on Creep and Fracture of Engineering Materials and Structures, Swansea, Great Britain, 1993, p. 255.
19. R. D. FIELD, T. M. POLLOCK and W. H. MURPHY, in "Superalloy 1992" edited by S. D. Antolovich et al. (Minerals, Metals & Materials Society, 1992) p. 557.
20. A. K. SINGH, N. LOUAT and K. SADANANDA, *Metall. Trans.* **19A** (1988) 2965.
21. J. X. ZHANG, T. MURAKUMO, Y. KOIZUMI and H. HARADA, submitted to *Metall Trans A.*
22. J. P. HIRTH and J. LOTHE, "Theory of Dislocations," 2nd ed. (Krieger Publishing Company, Malabar, FL, 1992).

Received 31 January
and accepted 14 August 2003